



Article

Hot-Spot Stress Analyses of a T-Shaped Tubular Joint Subjected to Uniform, Grooving and Non-uniform Corrosion

Lingsu Liu ¹, Yan Dong ^{1,2,3,*}, Haikun Yang ¹, Minghui Xu ¹, Xin Liu ¹ , Lei Zhang ¹ and Yordan Garbatov ^{3,4,*} 

¹ Yantai Research Institute, Harbin Engineering University, Yantai 261400, China; lsliu@hrbeu.edu.cn (L.L.); yhk@hrbeu.edu.cn (H.Y.); xmh947197004@hrbeu.edu.cn (M.X.); xin.liu@hrbeu.edu.cn (X.L.); zhanglei123@hrbeu.edu.cn (L.Z.)

² College of Shipbuilding Engineering, Harbin Engineering University, Harbin 150001, China

³ HEU-UL International Joint Laboratory of Naval Architecture and Offshore Technology, Harbin 150001, China

⁴ Centre for Marine Technology and Ocean Engineering (CENTEC), Instituto Superior Técnico, Universidade de Lisboa, 1649-003 Lisbon, Portugal

* Correspondence: yan.dong@hrbeu.edu.cn (Y.D.); yordan.garbatov@tecnico.ulisboa.pt (Y.G.)

Abstract: The study aims to investigate the impact of uniform, grooving and non-uniform corrosion degradation on the hot-spot stresses of a T-shaped tubular joint using the finite element method. The through-thickness linearization method is employed to estimate the hot-spot stresses, allowing a more reasonable consideration of the effect of grooving corrosion and non-uniform corrosion. The grooving corrosion degradation is modelled assuming that the corrosion rate of the weld metal is 1.4 times that of the base metal. The non-uniform corrosion is modelled by moving the nodes around the weld by a random distance along the direction perpendicular to the surface. The random distances are generated based on the surface roughness parameter R_a . The results indicate that the stress concentration factor (SCF) increases with the uniform corrosion depth. The grooving corroded tubular joint results in a higher SCF than those of the corresponding uniformly corroded tubular joint. The non-uniform corrosion can lead to SCF deviations from the SCF of the uniformly corroded tubular joint. The SCF deviation at the critical region follows the normal distribution, and its standard deviation increases with R_a .



Citation: Liu, L.; Dong, Y.; Yang, H.; Xu, M.; Liu, X.; Zhang, L.; Garbatov, Y. Hot-Spot Stress Analyses of a T-Shaped Tubular Joint Subjected to Uniform, Grooving and Non-uniform Corrosion. *Appl. Sci.* **2024**, *14*, 4812. <https://doi.org/10.3390/app14114812>

Received: 9 May 2024

Revised: 29 May 2024

Accepted: 31 May 2024

Published: 2 June 2024



Copyright: © 2024 by the authors. Licensee MDPI, Basel, Switzerland. This article is an open access article distributed under the terms and conditions of the Creative Commons Attribution (CC BY) license (<https://creativecommons.org/licenses/by/4.0/>).

Keywords: fatigue; grooving corrosion; non-uniform corrosion; hot-spot stress; tubular joint

1. Introduction

Ships and offshore structures are subjected to aggressive environments and cyclic loads, leading to fatigue and corrosion degradation and a reduction in structural safety [1]. It has been shown that the process of structural degradation caused by corrosion degradation and fatigue damage is complex. When corrosion protection measures fail, different types of corrosion degradation such as general, pitting, grooving and edge corrosion degradation may occur [2]. Corrosion degradation can lead to fatigue crack initiation because it increases local stress [3]. The increase in the local stress and the change in the fatigue crack growth characteristics also reduce the fatigue crack growth life [4–6]. External stress may also accelerate the corrosion rate, resulting in uneven corrosion degradation in high-stress areas around the welded joint, thus reducing the fatigue life of the structure [7].

The design standards consider the effect of corrosion degradation and fatigue in a straightforward way. When evaluating the local stress for the fatigue strength assessment, the component thickness is uniformly reduced by a certain amount. In addition, the S-N curve for the corrosion environment is recommended, which is obtained by reducing the in-air S-N curve with an environmental reduction factor [8].

Some studies have been performed to investigate the effects of corrosion on local stresses. Garbatov et al. [9] examined the influence of uniform corrosion wastage on the stress concentration factors (SCFs) of typical ship structural details and compared the

fatigue damage for different corrosion models. Yang et al. [7] investigated the accelerated corrosion degradation of highly stressed steel, and the time-dependent SCF as a function of corrosion deterioration was analysed considering the non-uniform corrosion of welded joints. Moan and Ayala-Uraga [4] established a reliability-based model for the assessment of deteriorating ships subjected to multiple environmental conditions. The model was based on a fracture mechanics formulation, and the corrosion-induced increased crack growth rate was considered in two aspects: (1) the increased stress range produced by the plate thinning (wastage) effect and (2) corrosion fatigue itself. Following the same strategy, Dong et al. [5] performed the fatigue reliability assessment of welded multi-planar tubular joints of the support structure of a fixed jacket offshore wind turbine considering the effect of corrosion and inspection.

Tubular joints are widely used in offshore structures and are prone to fatigue due to the high stress concentration. The stress concentration is quantified by the SCF defined as the ratio of the hot-spot stress of a point of the weld toe to the nominal stress, which depends on the joint type, geometric dimensions, and the loading type. Extensive studies have been performed to develop parametric equations for the calculation of SCFs of tubular joints. The Efthymiou equations are widely adopted in practice and incorporated into design codes [8]. Reviews on the SCFs of tubular joints can be found in [10–12].

The coating life is not considered, and the well-developed corrosion degradation phase is dealt with in the present study. In addition to the well-known uniform corrosion, the grooving and non-uniform corrosion are investigated. The grooving corrosion is referred to as preferential weld line corrosion degradation, with a localized line of material deterioration normally adjacent to welded joints long abutting stiffeners and at stiffener or plate butts or seams [2]. Incidents probably caused by grooving corrosion in a bulk carrier were reported [13]. Some studies have been performed to evaluate the effect of grooving corrosion on the ultimate strength of stiffened plate structures [14,15]. The effect of grooving corrosion on the load-bearing capacity of welded hollow spherical joints was investigated using the finite element method [16,17]. The grooving corrosion may also happen around the brace-to-chord weld of tubular joints, which can affect the SCFs. However, there are no detailed studies on the modelling of the grooving corrosion in the SCF analyses and on the effect of grooving corrosion on the SCFs of tubular joints.

Non-uniform corrosion refers to the phenomenon of uneven corrosion rates on surfaces of structural components. This may be due to the metal surface being affected by different environmental conditions, or due to the inhomogeneity of the metal material itself. Non-uniform corrosion may lead to more severe corrosion in the local area of metal components, reducing the strength and reliability of the components. It has been shown that the influence of non-uniform corrosion on the ultimate strength of tubular members cannot be ignored [18–20]. Shojai et al. [3,21] illustrated that the fatigue cracks were generally initiated from the region of the most significant stress concentration caused by pits and compared different modelling techniques to simulate the local stress concentration characteristics of pit corroded steel plate. The fatigue strength of tubular joints can be influenced by non-uniform corrosion. The local stress concentration can be accurately estimated using fine mesh finite element (FE) models, while the hot-spot stress was evaluated based on a coarse mesh. It is of interest to consider the effect of non-uniform corrosion using the hot-spot stress approach since it is used in practice.

In the present study, the effect of various forms of corrosion on the SCF of a T-shaped tubular joint is investigated using the FE method. The through-thickness linearization method instead of the surface extrapolation method is used to determine the hot-spot stress. The grooving corrosion is modelled assuming different corrosion rates between the weld metal and the base metal. The non-uniform corrosion is modelled based on the roughness of the structure surface. The SCFs for different corrosion conditions are evaluated.

2. Finite Element Model to Determine SCF

The FE model of a T-shaped tubular joint to determine the SCF is presented. The main feature of the model is that the geometry of the weld is included, so it can lead to more realistic results [12]. The modelling of the uniform, grooving and non-uniform corrosion is presented in the next section.

The geometry of the T-shaped tubular joint is illustrated in Figure 1. The values of geometrical parameters are in the range of application of Efthymiou equations recommended by DNV [8].

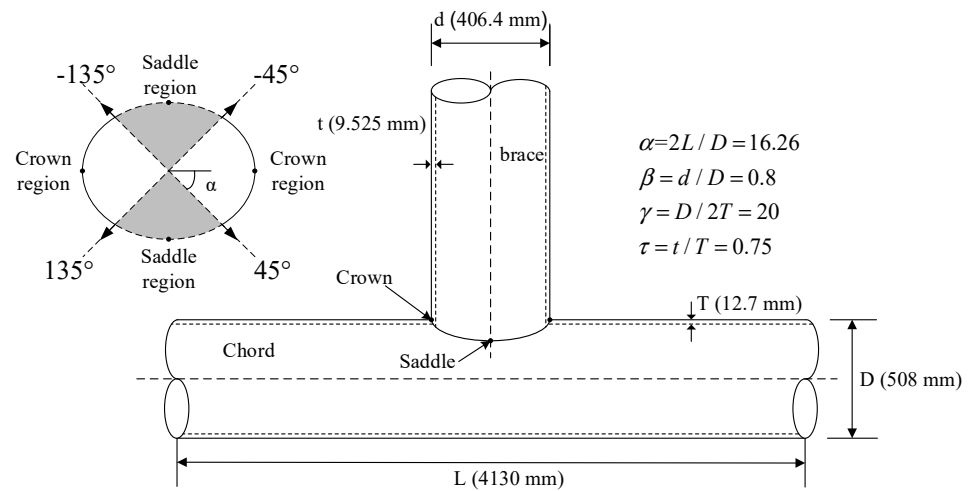


Figure 1. Geometry of T-shaped tubular joint.

Accurate modelling of the weld geometry is important for the determination of the SCF [22]. In the present study, the weld geometry along the intersection between the chord and brace is assumed based on the specifications of the AWS [23]. The dihedral angle ψ is defined as the angle between the chord and brace surface, which varies along the intersection curve. For the T-shaped tubular joint, ψ varies from 90° at the crown to $\pi - \cos^{-1}(\beta) \approx 143^\circ$ at the saddle [10]. The weld geometry specified by the AWS is closely related to ψ . Prequalified joint dimensions and groove angle for the tubular T joint are shown in Table 1. The joint details are shown in Figure 2. According to the requirements shown in Table 1, the following joint dimensions are assumed: $\omega = 45^\circ$, $R = 2$ mm, $c = 0$ mm, $F = t/2$, and $t_w = t$. The joint included angle is the difference between ψ and ω , which satisfies the requirement. The weld leg size can be less than $t/2$ for $\psi > 90^\circ$. A conservative assumption that F has a constant value equal to $t/2$ along the intersection curve is adopted to simplify the modelling.

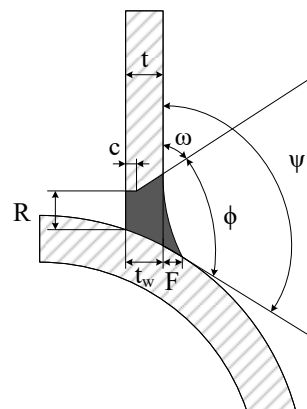


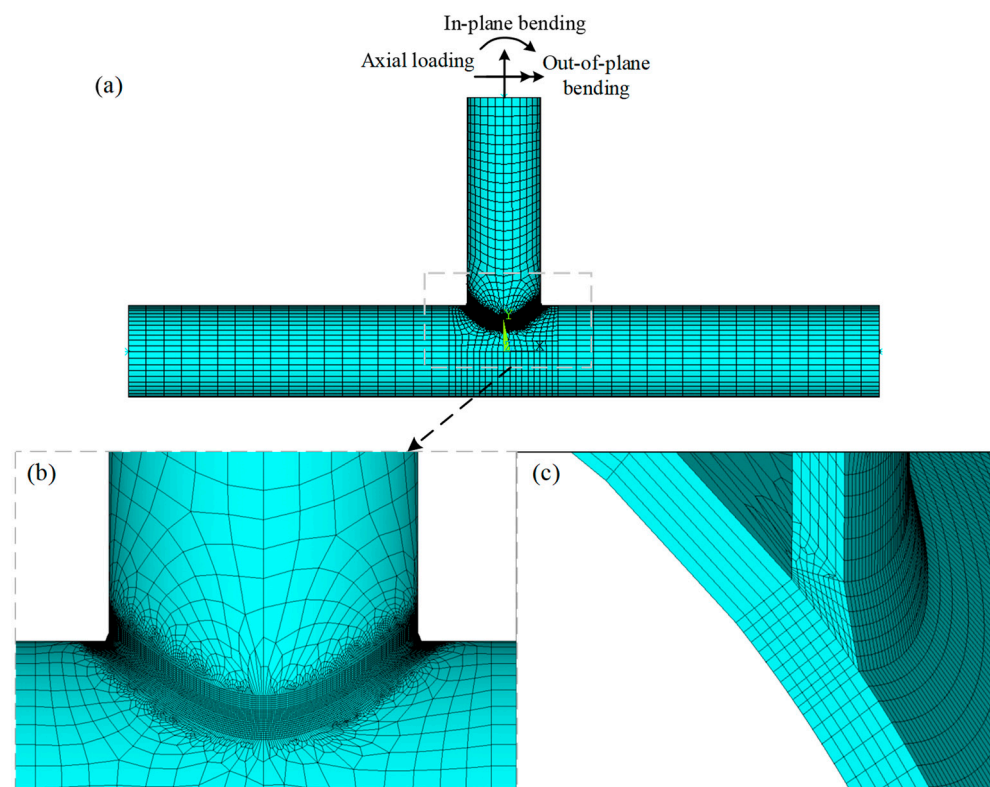
Figure 2. Joint details of the T-shaped tubular joint.

Table 1. Prequalified joint dimensions and groove angle for the T-shaped tubular joint with $90^\circ \leq \psi \leq 143^\circ$.

Parameter	Range
End preparation angle, ω	From 10° (or 45° for $\psi > 105^\circ$) to 90°
Root opening, R	From 2 mm to 6 mm
Root face, c	From 0 to 2 mm
Joint included angle, φ	From 37.5° to 60° for $\psi \leq 105^\circ$ Not less than 37.5° for $\psi > 105^\circ$
Weld leg size, F	From 0 to $t/2$ as ψ varies from 135° to 90°
Weld thickness, t_w	Not less than t

2.1. Finite Element Model

The FE analyses are performed using ANSYS Mechanical APDL 2020 R2 [24]. The element type SOLID186 is used. The mesh condition is shown in Figure 3. The FE model is divided into several zones. Coarse mesh is used in the zone away from the weld, and in the zone including the weld, dense mesh is employed. A mesh convergent study is conducted to justify the mesh condition. The number of elements for the thickness of the chord and brace is 6, where 648 elements are used along the intersection curve of the weld toe. The approximate mesh size around the weld toe is 2 mm. Young's modulus and Poisson's ratio are 206 GPa and 0.3, respectively. Both chord ends are fixed, and the three load cases acting on the brace are considered, namely axial loading, in-plane bending and out-of-plane bending.

**Figure 3.** Mesh distribution of the tubular joint: (a) global view; (b) around the intersection; (c) around the weld toe.

2.2. Hot-Spot Stress

The SCF is calculated as the ratio between the hot-spot stress at the weld toe and the nominal brace stress. The surface stress extrapolation method is used to determine hot-spot stress. However, for the grooving corrosion, the surface stress of the chord near

the weld toe is not monotonic when approaching the weld toe. There is a decrease and subsequent increase in the stress component perpendicular to the weld toe, so the use of the surface extrapolation method may be questionable [25]. Additionally, for the non-uniform corrosion degradation condition, because the stress concentration is more localized, the stress at the reference points of the surface stress extrapolation method cannot reflect the stress at the weld toe. Therefore, in the present study, the through-thickness linearization method is used to determine the hot-spot stress.

The stress distribution along the weld toe section can be separated into three components, namely the membrane stress, bending stress and nonlinear stress [26]. The peak stress σ_{peak} at the weld toe is the summation of the three components. The hot-spot stress is the summation of the membrane stress σ_{hs}^m and the bending stress σ_{hs}^b , as shown in Figure 4.

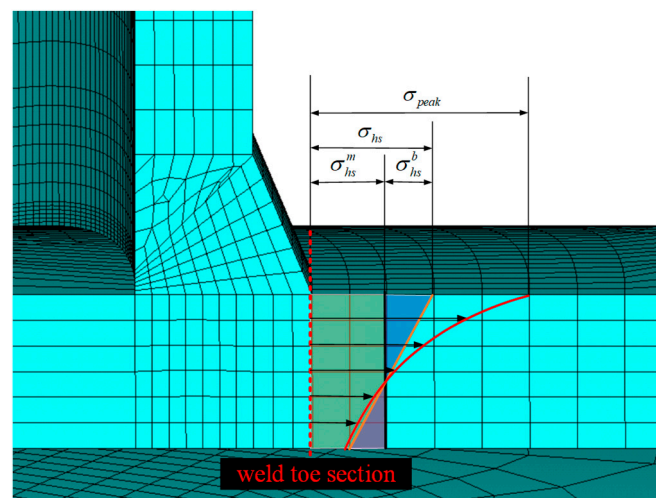


Figure 4. The stress field in the critical section of the welded toe.

The stress linearization at the weld toe section can be carried out by ANSYS. The path along the thickness direction is defined in the section. By defining the local coordinate system, the stress component perpendicular to the weld toe section is obtained for all the nodes on the path. The membrane stress and bending stress are calculated automatically.

To validate the FE analysis method, the obtained SCF results are compared with the experimental results provided by Yeoh et al. [27] and Soh [28] and the results of Efthymiou equations [8], as shown in Figure 5. Although the experimental method is based on the surface stress extrapolation method, the results obtained by FE analyses using the through-thickness linearization method are consistent with the experimental results. The shape of the SCF distribution from the experimental measurement is well captured. In the case of axial loading and IPB, there are some differences at the crown, which is reasonable, because the strain gauge failed to provide accurate information about the position of the weld toe and weld geometry in the experiment, and some measurement inaccuracies have been reported [27]. Compared with Efthymiou equations, the SCF calculated by the FE method at the saddle is underestimated under axial loading and IPB, while the SCF of the crown is slightly overestimated. This error may be due to the modelling of the weld geometry in the FE method, which is not considered in the development of the Efthymiou equations.

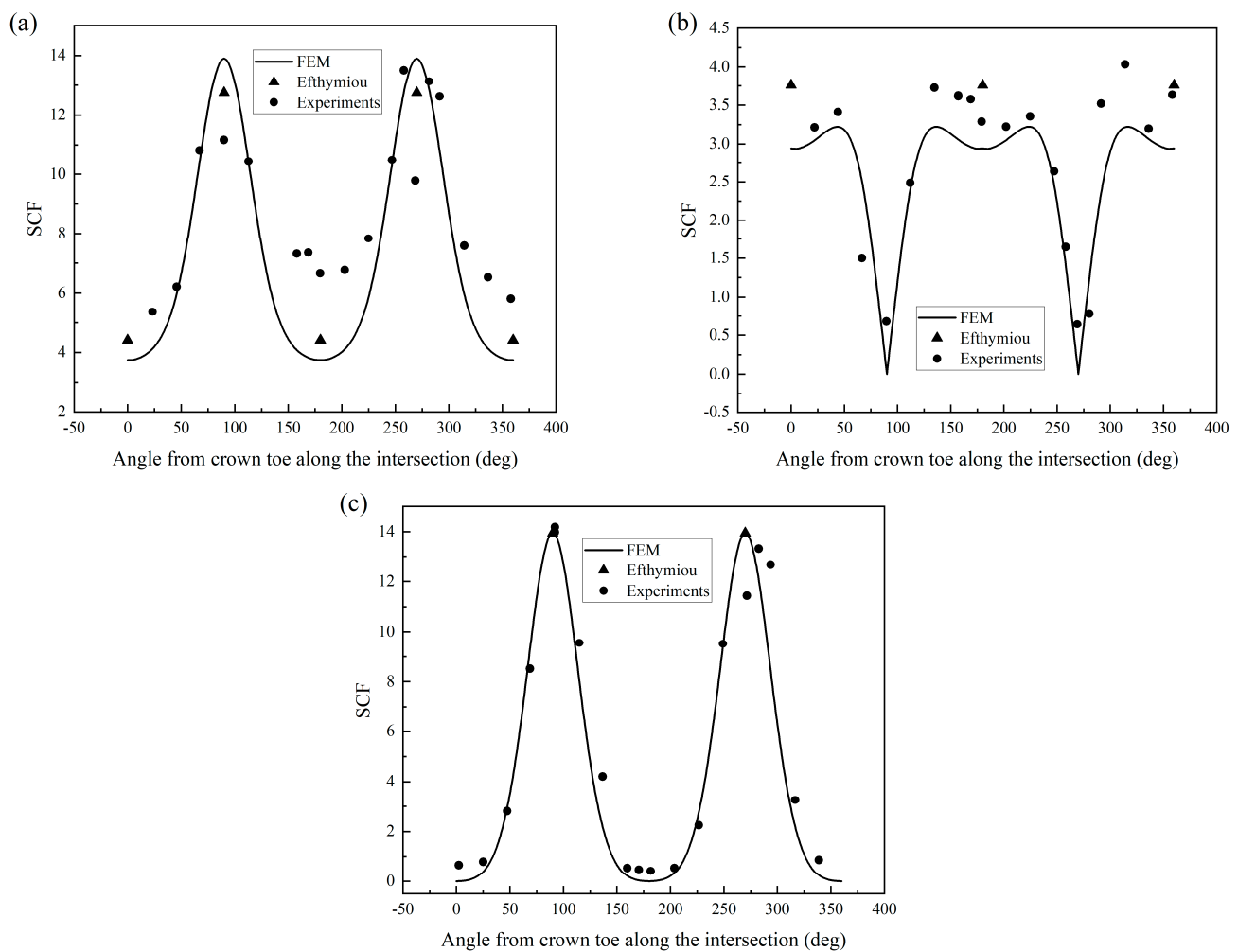


Figure 5. SCFs of weld toe on the chord under (a) axial loading; (b) in-plane bending (IPB); and (c) out-of-plane bending (OPB).

3. Corrosion Modelling

3.1. Uniform and Grooving Corrosion

The grooving corrosion mechanism was investigated by Kato et al. [29]. Rapid heating and cooling of welding can produce a sulphide-enriched portion surrounding the MnS inclusions, which dissolves anodically concerning MnS inclusions and the base metal. Corrosion pits were initiated immediately on the MnS inclusions. They were then developed into grooving corrosion with the aid of the macro-cell between the anodic weld and cathodic base metal. In addition, the protective coating around the weld may not be as good as that on the base metal because of the existence of weld defects, which can lead to localized grooving corrosion [14]. The grooving corrosion can also be attributed to an unfavourable local corrosive environment and the residual stress caused by welding, which leads to stress corrosion degradation and a greater corrosion depth around the weld than that away from the weld [16]. The high stress arising at the hot spot caused by external loading can also accelerate the corrosion degradation rate and lead to non-uniform corrosion [7]. Tanaka et al. [30] conducted some continuous immersion tests in seawater and found that the grooving corrosion occurring on welded joints is the consequence of galvanic corrosion and stress corrosion.

The uniform corrosion and grooving corrosion are modelled as shown in Figure 6. The outer surface of the tubular joint is uniformly removed due to uniform corrosion whose corrosion depth is d . The modelling of grooving corrosion is mainly based on the work of Tanaka et al. [30]. It is assumed that the weld metal and base metal are both subjected to

uniform corrosion, but their corrosion rates are different; the corrosion rate of weld metal is 1.4 times that of the base metal, i.e., the corrosion depth of the weld metal d_g equals 1.4 d . The above assumptions are consistent with the observations in [30]. The corrosion degradation rate of the heat-affected zone is assumed to be linearly varied from the weld metal to the base metal, and the width of the heat-affected zone b_g is assumed to be 3 mm. It has been shown that plastic deformation is the main reason for stress corrosion [30]. Because plastic deformation is limited in practice, the contribution of stress corrosion to grooving corrosion is ignored. The reference points for the determination of the hot-spot stress are placed concerning the new weld toe and plate thickness due to corrosion. The FE models of uniform and grooving corrosion are shown in Figure 7.

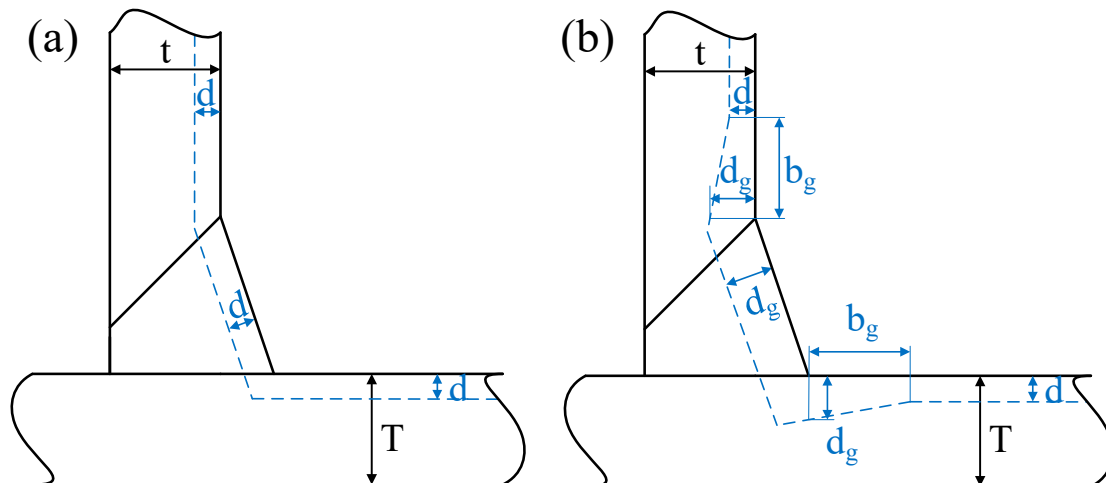


Figure 6. Modelling of (a) uniform corrosion and (b) grooving corrosion.

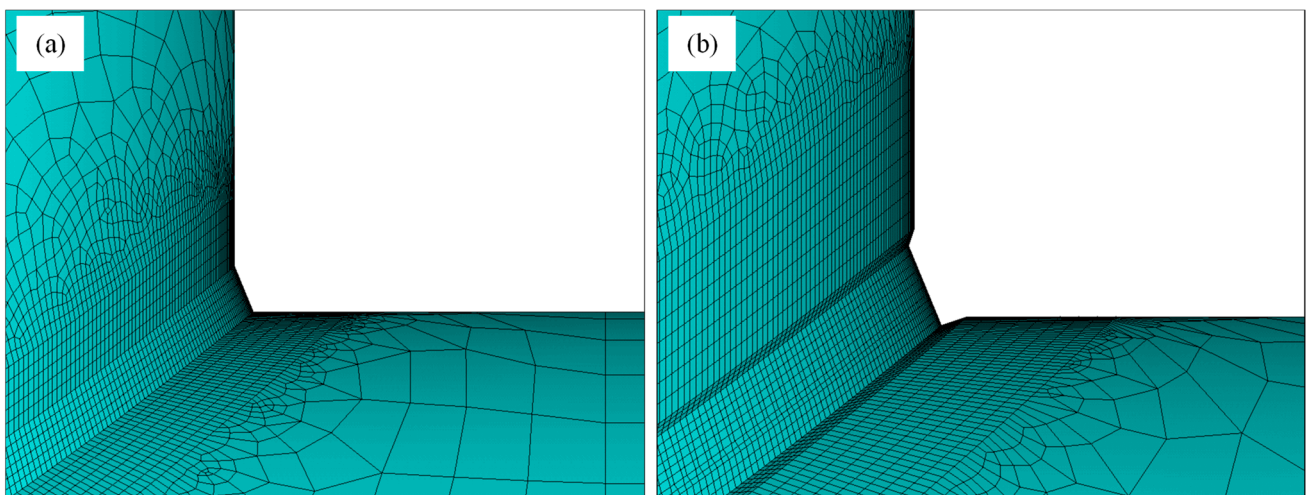


Figure 7. FE model of (a) uniform corrosion and (b) grooving corrosion.

3.2. Non-Uniform Corrosion

It was suggested by Woloszyk and Garbatov [31] that general corrosion causes degradation on two levels: the reduction in the mean thickness and local irregularities on the surfaces of corroded elements. The local irregularities can be further divided into global non-uniformity and micro non-uniformity. The former can be captured by a very dense measurement grid, but the latter cannot be captured because their size is smaller than the sizes of measuring probes.

In the present study, the local irregularities on the mesh size level are considered. The mesh size for hot-spot stress analyses is around 2 mm. More localized irregularities are

ignored. The uniform corroded tubular joint is modelled at first. Then the nodes around the weld are moved upward or downward along the direction perpendicular to the surface. The moving distance and direction of these nodes follow a sample of a normally distributed random variable with a mean value of zero. The standard deviation of the random variable is derived from the roughness parameter Ra . The definition of Ra is as follows:

$$Ra = \frac{1}{l_r} \int_0^{l_r} |z(x)| dx \quad (1)$$

where l_r is the evaluation length, and z is the vertical coordinates of the corroded surface concerning the mean surface. Assuming z is a normally distributed random variable with a mean value of zero, the absolute value of z follows a half-normal distribution. The mean value of the half-normal distribution, which equals Ra , is as follows [32]:

$$Ra = \sigma \sqrt{2/\pi} \quad (2)$$

where σ is the standard deviation of z . If the roughness of a corroded surface is known, σ can be derived from Equation (2). A sample can be generated based on the normal distribution of $N(0, \sigma)$. The non-uniform corroded FE model is obtained by moving the nodes around the weld. An example of the non-uniform corroded FE model is shown in Figure 8.

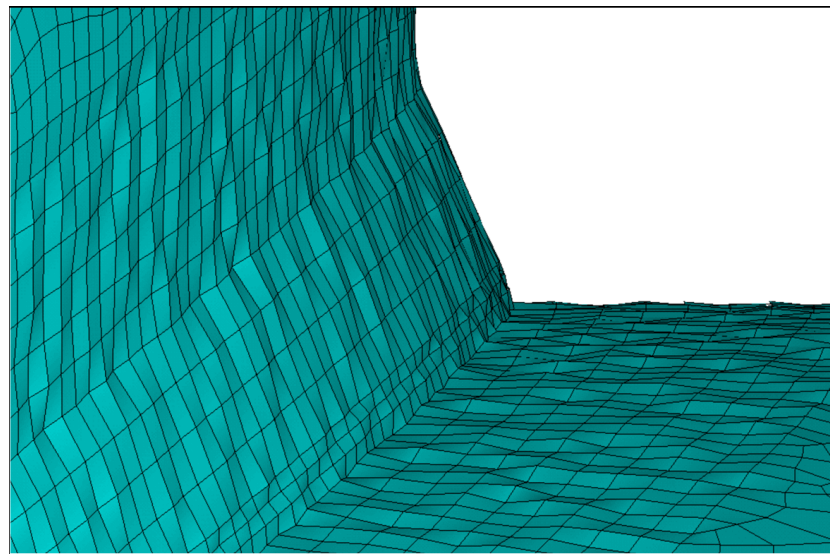


Figure 8. Non-uniform corroded FE model.

The relationship between the roughness and corrosion time is approximated using measured data. The Ra values of steel plates for 2 years and 5 years of exposure time in a real marine environment were measured by Gkatzogiannis et al. [33] and Xia et al. [34]. Xia et al. [34] obtained Ra values from three samples exposed to an underwater environment for 5 years. The average of the three Ra values and the Ra value for 2 years of exposure time obtained by Gkatzogiannis [33] are used for the regression. The uncertainty of Ra is not considered in the present study. A linear relationship between Ra and the corrosion time is assumed, and a straight line is fitted based on the data as shown in Figure 9.

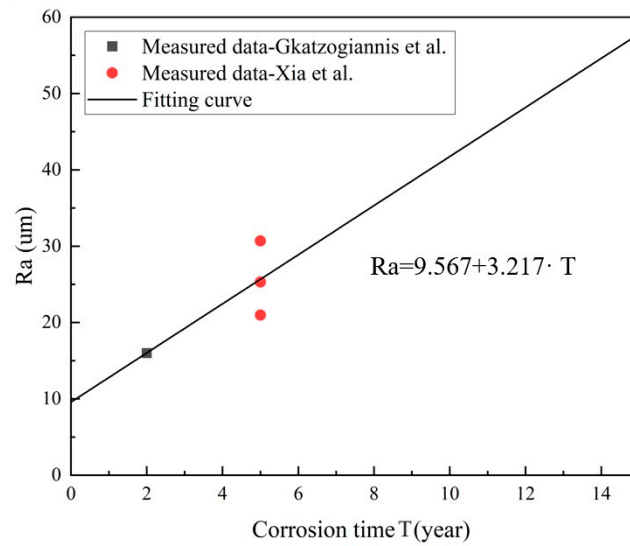


Figure 9. Ra as a function of corrosion time T, Gkatzogiannis et al. [33] and Xia et al. [34].

4. Results

4.1. Effect of Uniform Corrosion

The effect of uniform corrosion degradation on the SCFs is shown in Figure 10. The corrosion depth *d* ranges from 0 to 2.5 mm. Using a corrosion rate of 0.1 mm/year [30] and a service life of 25 years, the maximum uniform corrosion depth is 2.5 mm. Figure 10 shows the variation of the SCFs at the critical points as a function of the uniform corrosion depth. The SCFs are calculated using the FE method and the Efthymiou equations, respectively.

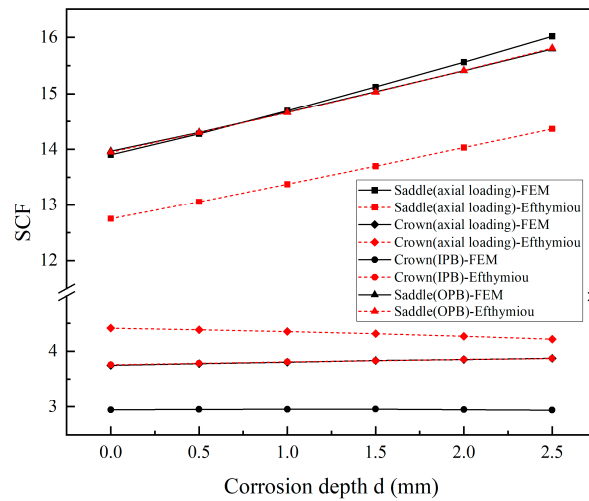


Figure 10. SCFs as a function of uniform corrosion depth.

The FE results show that the SCFs increase with *d*, and the effects of *d* on the SCFs are linear. The effects of uniform corrosion on the SCFs cannot be neglected. The effects of *d* on the SCFs depend on the loading condition and the location. For the SCF of the saddle, the effect of *d* on the SCF of the saddle is significant. Under axial loading, the SCF of the saddle increases by 16%, and under OPB, the SCF of the saddle increases by 14%. For the SCF of the crown, *d* has a small impact on the SCF of the crown, especially in the case of IPB.

Although the results of the Efthymiou equations deviate from those of the FE method, similar trends with the corrosion depth are observed. For the case of axial loading, the SCF of the crown slightly decreases with the increase in *d*, which is not consistent with the FE results. The other SCFs are all increased with *d*. Compared with the FE results, the Efthymiou equations slightly underestimate the increase in the SCFs for the saddle under

axial loading when d becomes large. The difference in the results of FE and Efthymiou equations may be partly attributed to the different thinning strategies of the two methods. In the FE method, it is assumed that the corrosion degradation does not happen at the interior region, and the material inside the brace including the part material located at the outer surface of the chord remains unchanged. It is assumed that the thicknesses of the chord and brace are both reduced uniformly when using the Efthymiou equations.

4.2. Effect of Grooving Corrosion

For the grooving corroded tubular joint, the results of the surface stress extrapolation method are compared with those of the through-thickness linearization method for the axial loading condition. The SCFs as a function of d are shown in Figure 11. The trends of SCFs are different. The SCFs obtained by the surface stress extrapolation method decrease with d , and the decrease is not continuous, while the SCFs obtained by the through-thickness linearization method continuously increase with d . The difference in the SCF between the two methods becomes significant when d varies from 0 to 2.5 mm.

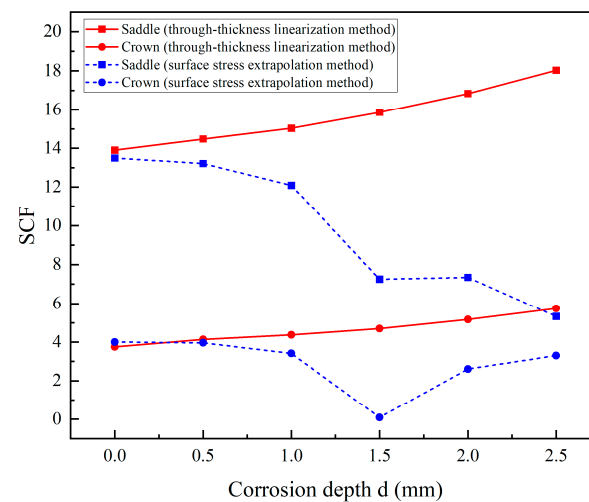


Figure 11. Thickness linearization method and surface stress extrapolation method.

It has been observed that surface stress typically increases approaching the weld toe, and the stress at the first reference point (0.4 T) is higher than at the second reference point (1.0 T). However, in the case of grooving corrosion degradation, the increasing surface stress is subjected to a decrease and subsequent increase when approaching the weld toe [25]. As a result, the stress at the first reference point is lower than that at the second reference point for some cases. The use of the surface extrapolation method to determine hot-spot stresses can yield lower SCFs. When employing a surface stress extrapolation, it is assumed that the nonlinear component has effectively disappeared on the plate surface at a distance greater than 0.4 T from the weld toe, and stress and strain increase almost linearly near the weld toe [26]. However, the complex stress distribution and the inconsistency with the assumption for grooving corrosion conditions pose challenges to the use of the surface extrapolation method. The use of the through-thickness linearization method is more reasonable for grooving corrosion degradation conditions.

By using the through-thickness linearization method, the SCFs are obtained for various corrosion depths, as shown in Figure 12. The SCFs of critical locations are all increased with corrosion depth. Under axial loading and OPB, the maximum SCF always appears at the saddle, and the minimum SCF always appears at the crown. However, under IPB, the SCF distribution along the intersection changes with corrosion depth. The maximum SCF appears between the saddle and crown when there is no corrosion degradation at the tubular joint or under uniform corrosion degradation conditions. However, for grooving corrosion conditions, as the corrosion depth d increases, the position of the maximum hot-spot stress gradually shifts to the saddle.

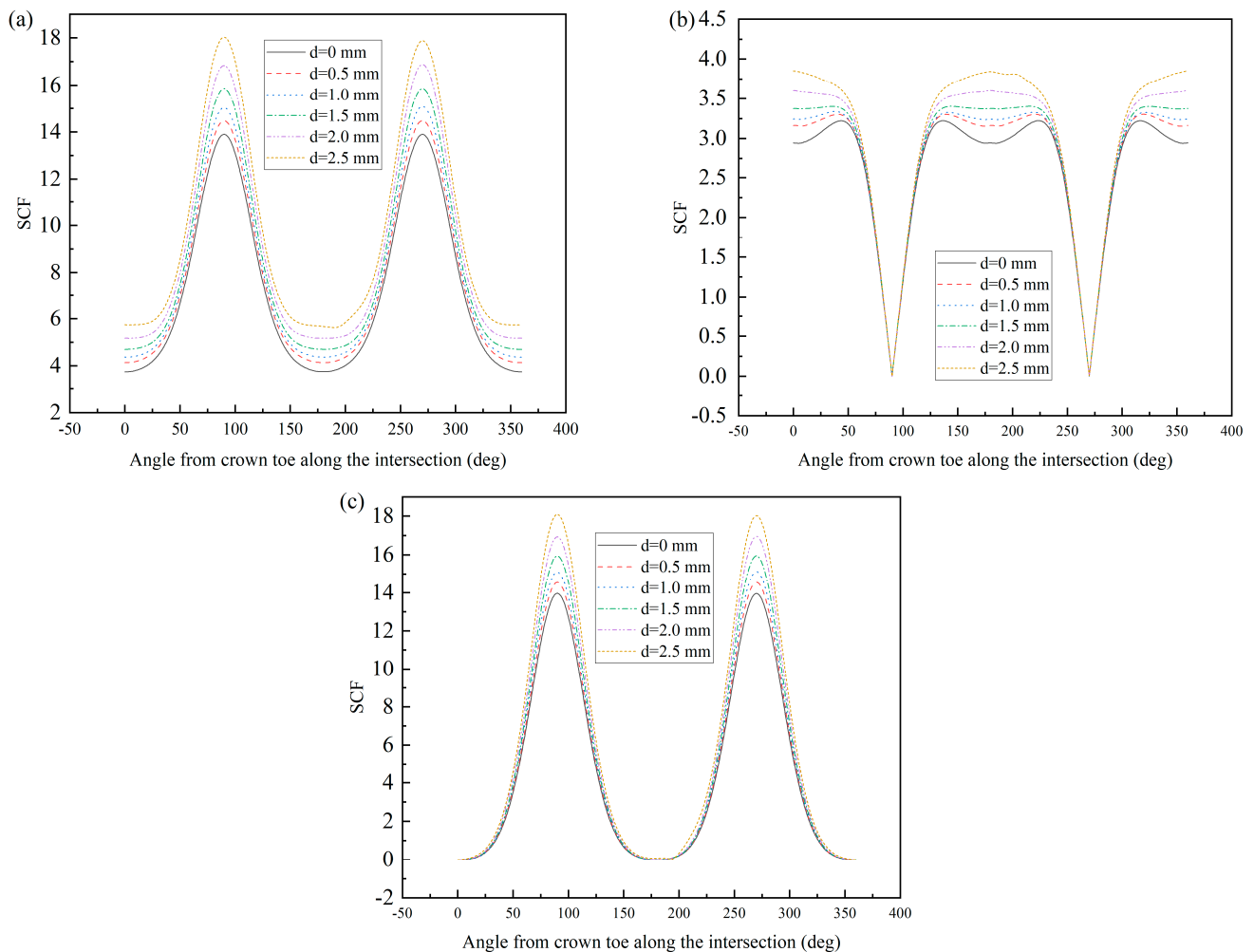


Figure 12. SCFs of the weld toe on the chord for grooving corrosion under (a) axial loading; (b) in-plane bending; and (c) out-of-plane bending.

The results of the grooving corrosion cases are compared with those of the uniform corrosion cases, as shown in Figure 13. In contrast to the linear increase in the SCF with d for uniform corrosion cases, the SCF increases nonlinearly with d for grooving corrosion cases. Compared with uniform corrosion degradation, grooving corrosion results in higher SCFs. Therefore, grooving corrosion is more detrimental than uniform corrosion for the tubular joint, and the remaining fatigue life is significantly reduced.

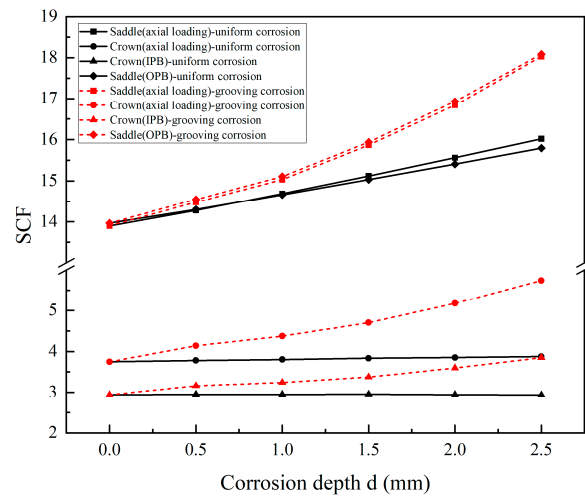


Figure 13. SCFs between grooving corrosion and uniform corrosion.

4.3. Effect of Non-Uniform Corrosion

The uniformly corroded tubular joint and 10 non-uniformly corroded tubular joints are analysed under axial loading, and the SCFs are compared to illustrate the effect of non-uniform corrosion degradation as shown in Figure 14. The exposure time of these joints is assumed to be 15 years, resulting in $d = 1.5$ mm (corrosion rate 0.1 mm/year) and $Ra = 57.822$ μm based on the linear equation shown in Figure 9. Non-uniform corrosion can result in significant fluctuation of the hot-spot stress around the uniform corrosion results. The SCF can be underestimated if only the uniform corrosion is considered.

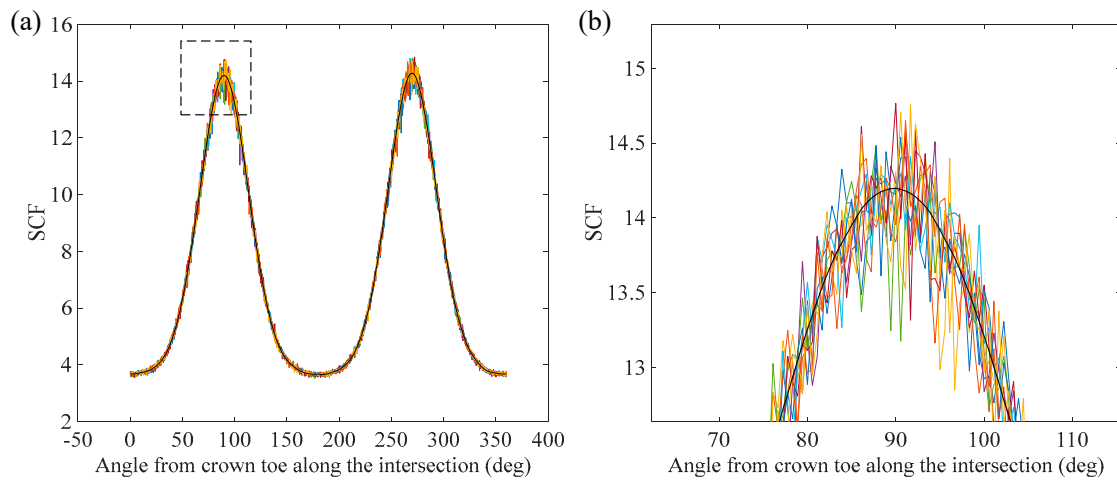


Figure 14. (a) SCF distributions along the intersection and (b) partial enlarged SCF distribution for the uniformly corroded tubular joint with $d = 1.5$ mm (black line) and 10 non-uniformly corroded tubular joints with $Ra = 57.822$ μm (other lines) under axial loading.

The SCF deviation caused by non-uniform corrosion is statistically analysed. The crown toe along the intersection is divided into four regions: two crown regions and two saddle regions [11], as shown in Figure 1. The SCF deviation for each weld toe node in the critical region where the maximum SCF appears is obtained as follows:

$$x_i = SCF_{nu,i} - SCF_{u,i} \tag{3}$$

where x_i is the SCF deviation of weld toe node i , $SCF_{nu,i}$ is the SCF of the non-uniformly corroded tubular joint at the node, and $SCF_{u,i}$ is the SCF of the uniformly corroded tubular joint at the node. Statistical analyses can be conducted based on the results for all the

nodes in the critical region. It has been found that the SCF deviation conforms to normal distributions. The SCF deviation at the critical region can be described by a normal distributed random variable. Normal distributions are regressed for the exposure time of 1, 2, 5, 10 and 15 years, respectively. The regressed distributions for various conditions are shown in Figure 15. The mean values of the SCF deviation are close to zero, and the standard deviation of the SCF deviation increases with the exposure time.

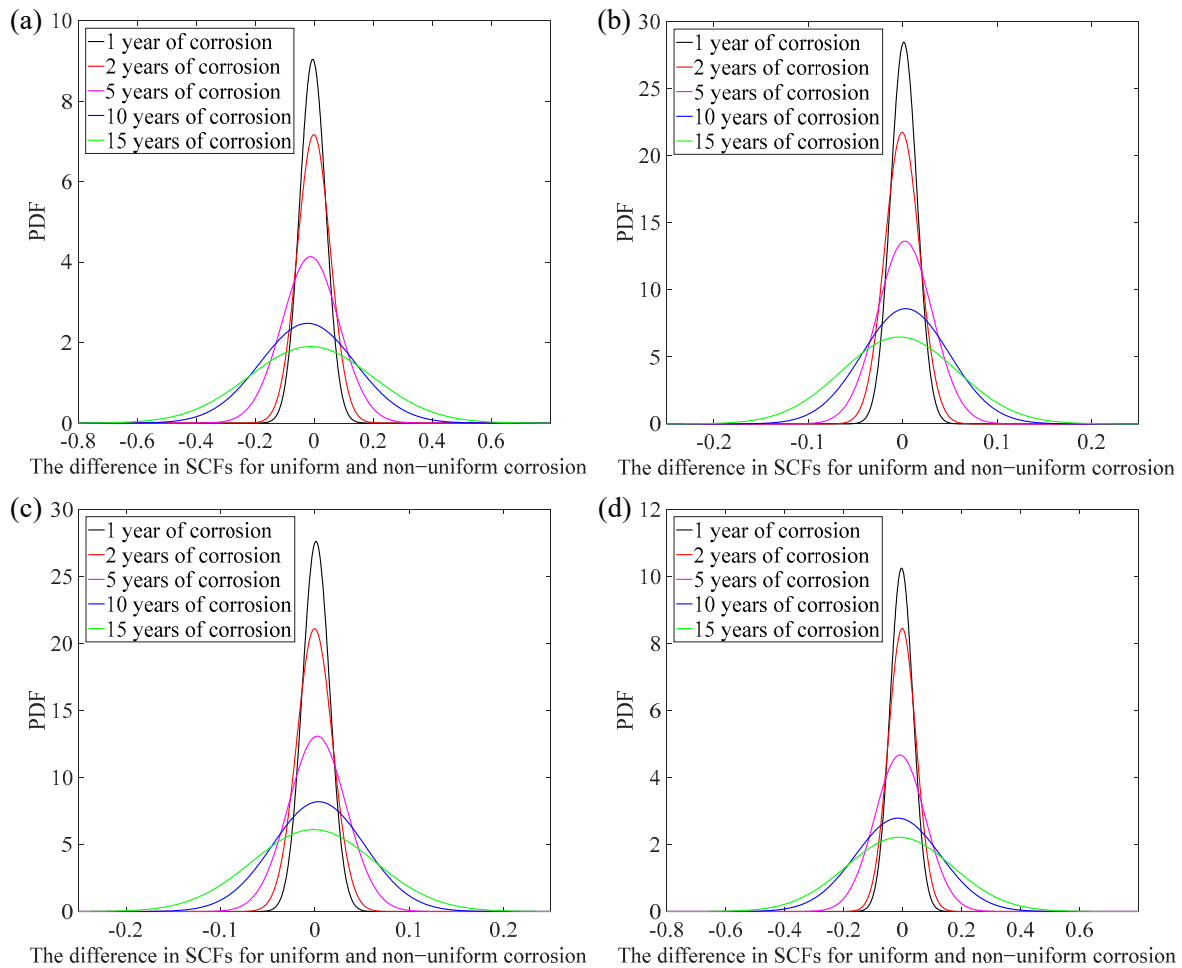


Figure 15. PDF of the SCF deviation between uniform and non-uniform corrosion: (a) saddle region under axial loading; (b) crown region under axial loading; (c) crown region under IPB; (d) saddle region under OPB.

The relationship between the standard deviation of the SCF deviation σ_χ and R_a is investigated. The σ_χ for the saddle region under axial loading, crown region under IPB and saddle region under OPB are evaluated, and the results are shown in Figure 16. It can be seen that σ_χ increases with R_a , and the relationship between σ_χ and R_a is approximately linear for all three loading conditions. The variation of σ_χ to R_a depends on the loading conditions.

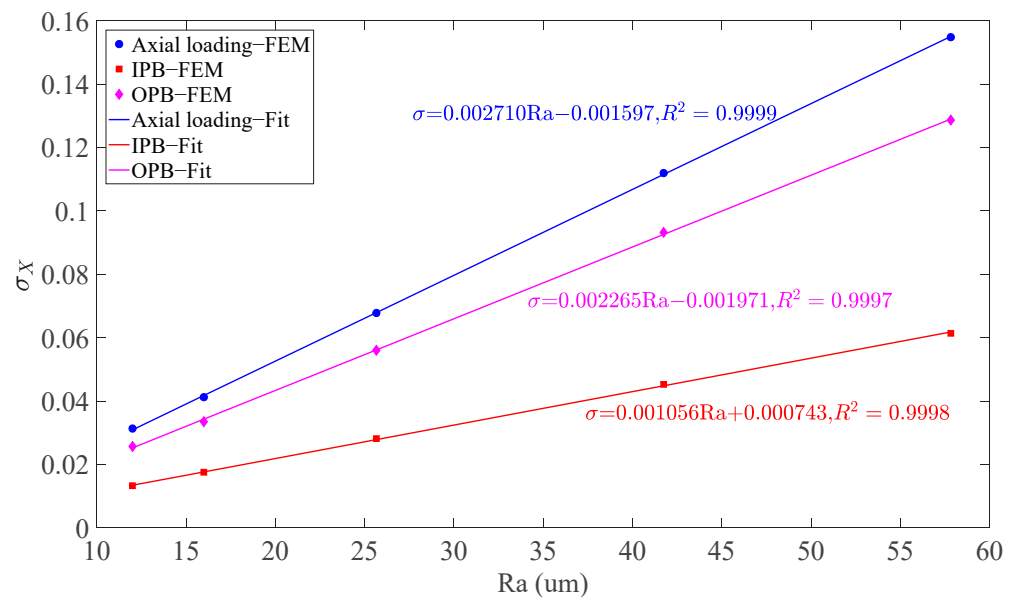


Figure 16. Relationship between standard deviation of SCF deviation and roughness.

The analyses of the non-uniformly corroded tubular joint are time-consuming because of the complex modelling procedures. To obtain a conservative maximum SCF only accounting for non-uniform corrosion, the following equation is proposed:

$$SCF_c = SCF_u + 2\sigma_X \tag{4}$$

where SCF_c and SCF_u are the maximum SCF accounting for the non-uniform corrosion and the maximum SCF of the uniformly corroded tubular joint, respectively. $2\sigma_X$ indicates that the exceeding probability is about 2.3%.

5. Conclusions

The effect of uniform, grooving and non-uniform random corrosion on the hot-spot stress of a T-shaped tubular joint was investigated using the FE method. The following conclusions can be established:

The FE model takes the weld geometry into account. The FE results are in good agreement with the experimental results and results from empirical equations. The uniform corrosion increases the SCFs, and the influence depends on the loading condition and the location. The SCF variations due to uniform corrosion predicted by the FE method are slightly different from those predicted by empirical equations.

The grooving corrosion is modelled such that the corrosion rate of the weld metal is 1.4 times that of the base metal. For the grooving corrosion conditions, the SCFs obtained by the surface stress extrapolation method decrease with the increase in corrosion depth due to the complex stress distribution when approaching the weld toe, making the method questionable. For the grooving corrosion conditions, the through-thickness linearization method is more appropriate. The SCFs of grooving corroded tubular joints are higher than the corresponding uniform corroded tubular joints. The grooving corrosion is more detrimental than uniform corrosion for the tubular joint.

The non-uniform corrosion is modelled based on the roughness parameter which increases with exposure time. The SCF of the non-uniformly corroded tubular joint fluctuated around the SCF of the uniformly corroded one. The SCF deviation at the critical region can be described by a normal distributed random variable. The standard deviation of the SCF deviation has a linear relationship with the roughness parameter. A simple method is proposed to account for the effect of non-uniform corrosion on the maximum SCF of the tubular joint.

Note that the modelling of the grooving and non-uniform corrosion degradation is an idealization of the real condition. The deviation of the results due to the idealization should be investigated in the future.

Author Contributions: Conceptualization, Y.D.; methodology, Y.D., L.L., H.Y., X.L. and L.Z.; validation, L.L. and H.Y.; formal analysis, L.L. and M.X.; investigation, L.L., H.Y. and M.X.; writing—original draft preparation, L.L., Y.D., X.L. and L.Z.; writing—review and editing, Y.G. All authors have read and agreed to the published version of the manuscript.

Funding: The present work is supported by the National Natural Science Foundation of China (Grant No. 52101350).

Institutional Review Board Statement: Not applicable.

Informed Consent Statement: Not applicable.

Data Availability Statement: The original contributions presented in the study are included in the article, further inquiries can be directed to the corresponding authors.

Conflicts of Interest: The authors declare no conflicts of interest.

References

1. Guedes Soares, C.; Garbatov, Y. Reliability of maintained ship hulls subjected to corrosion and fatigue under combined loading. *J. Constr. Steel Res.* **1999**, *52*, 93–115. [CrossRef]
2. DNV. Allowable Thickness Diminution for Hull Structure. 2014, Classification Note No. 72.1. Available online: <http://www.lloydsbritishegyptgroups.com/PDF/DNV.pdf> (accessed on 8 May 2024).
3. Shojai, S.; Schaumann, P.; Braun, M.; Ehlers, S. Influence of pitting corrosion on the fatigue strength of offshore steel structures based on 3D surface scans. *Int. J. Fatigue* **2022**, *164*, 107128. [CrossRef]
4. Moan, T.; Ayala-Uraga, E. Reliability-based assessment of deteriorating ship structures operating in multiple sea loading climates. *Reliab. Eng. Syst. Saf.* **2008**, *93*, 433–446. [CrossRef]
5. Dong, W.; Moan, T.; Gao, Z. Fatigue reliability analysis of the jacket support structure for offshore wind turbine considering the effect of corrosion and inspection. *Reliab. Eng. Syst. Saf.* **2012**, *106*, 11–27. [CrossRef]
6. Han, X.; Yang, D.Y.; Frangopol, D.M. Probabilistic life-cycle management framework for ship structures subjected to coupled corrosion–fatigue deterioration processes. *J. Struct. Eng.* **2019**, *145*, 04019116. [CrossRef]
7. Yang, S.; Yang, H.; Liu, G.; Huang, Y.; Wang, L. Approach for fatigue damage assessment of welded structure considering coupling effect between stress and corrosion. *Int. J. Fatigue* **2016**, *88*, 88–95. [CrossRef]
8. DNVGL. Fatigue Design of Offshore Steel Structures. Recommended Practice DNVGL-RP-C203 2019, DNVGL-RP-C203. Available online: <https://www.dnv.com/oilgas/download/dnv-rp-c203-fatigue-design-of-offshore-steel-structures/> (accessed on 8 May 2024).
9. Garbatov, Y.; Rudan, S.; Guedes Soares, C. Fatigue damage of structural joints accounting for nonlinear corrosion. *J. Ship. Res.* **2002**, *46*, 289–298. [CrossRef]
10. Ahmadi, H.; Lotfollahi-Yaghin, M.A.; Yong-Bo, S.; Aminfar, M.H. Parametric study and formulation of outer-brace geometric stress concentration factors in internally ring-stiffened tubular KT-joints of offshore structures. *Appl. Ocean Res.* **2012**, *38*, 74–91. [CrossRef]
11. Hectors, K.; De Waele, W. A numerical framework for determination of stress concentration factor distributions in tubular joints. *Int. J. Mech. Sci.* **2020**, *174*, 105511. [CrossRef]
12. Hectors, K.; De Waele, W. Influence of weld geometry on stress concentration factor distributions in tubular joints. *J. Constr. Steel Res.* **2021**, *176*, 106376. [CrossRef]
13. DNV. Incident Information on Grooving Corrosion on Ship’s Side. Available online: <https://officerofthewatch.com/2013/11/29/incident-information-on-grooving-corrosion-on-ships-side/> (accessed on 29 November 2013).
14. Wang, Y.; Wharton, J.A.; Shenoi, R.A. Ultimate strength assessment of steel stiffened plate structures with grooving corrosion damage. *Eng. Struct.* **2015**, *94*, 29–42. [CrossRef]
15. Zhu, Y.; Zhang, Y.; Du, F. Ultimate Strength of Hull Structural Stiffened Plate with Grooving Corrosion Damage under Uniaxial Compression. *J. Ship. Res.* **2021**, *65*, 309–319. [CrossRef]
16. Chen, H.; Liu, H.; Chen, Z. Compressive strength of corroded special-shaped welded hollow spherical joints based on numerical simulation. *Thin-Walled Struct.* **2020**, *149*, 106531. [CrossRef]
17. Chen, H.; Liu, H.; Chen, Z. Failure pressure of welded hollow spherical joints containing grooving corrosion defects and wall reduction. *Int. J. Steel Struct.* **2021**, *21*, 35–51. [CrossRef]
18. Li, G.; Hou, C.; Shen, L.; Yao, G.-H. Performance and strength calculation of CFST columns with localized pitting corrosion damage. *J. Constr. Steel Res.* **2022**, *188*, 107011. [CrossRef]

19. Wang, R.; Guo, H.; Sheno, R.A. Experimental and numerical study of localized pitting effect on compressive behaviour of tubular members. *Mar. Struct.* **2020**, *72*, 102784. [[CrossRef](#)]
20. Chen, B.-Q.; Zhang, X.; Guedes Soares, C. The effect of general and localized corrosions on the collapse pressure of subsea pipelines. *Ocean Eng.* **2022**, *247*, 110719. [[CrossRef](#)]
21. Shojai, S.; Schaumann, P.; Brömer, T. Probabilistic modelling of pitting corrosion and its impact on stress concentrations in steel structures in the offshore wind energy. *Mar. Struct.* **2022**, *84*, 103232. [[CrossRef](#)]
22. Dong, Y.; Garbatov, Y.; Guedes Soares, C. Recent Developments in Fatigue Assessment of Ships and Offshore Structures. *J. Mar. Sci. Appl.* **2022**, *21*, 3–25. [[CrossRef](#)]
23. AWS. Structural Welding Code: AWS D1.1. 2020. Available online: <https://istasazeh-co.com/wp-content/uploads/2022/02/AWS-D1.1-D1.1M-2020.pdf> (accessed on 8 May 2024).
24. ANSYS. Online Manuals. 2012. Available online: <https://lsdyna.ansys.com/manuals/> (accessed on 8 May 2024).
25. Dong, Y.; Liu, L.; Yang, H.; Garbatov, Y.; Liu, X. Impact of Uniform and Grooving Corrosion on Hot-spot Stresses of a T-Shaped Tubular Joint. In Proceedings of the International Conference on Maritime Technology and Engineering, Lisbon, Portugal, 14–16 May 2024.
26. Hobbacher, A. *Recommendations for Fatigue Design of Welded Joints and Components*; Springer: Berlin/Heidelberg, Germany, 2015.
27. Yeoh, S.-K.; Soh, A.-K.; Soh, C.-K. Behaviour of tubular T-joints subjected to combined loadings. *J. Constr. Steel Res.* **1995**, *32*, 259–280. [[CrossRef](#)]
28. Soh, A.-K. An improved procedure for the determination of hot spot stresses in tubular joints. *Fatigue Fract. Eng. Mater. Struct.* **1997**, *20*, 1709–1718. [[CrossRef](#)]
29. Kato, C.; Ootoguro, Y.; Kado, S.; Hisamatsu, Y. Grooving corrosion in electric resistance welded steel pipe in seawater. *Corros. Sci.* **1978**, *18*, 61–74. [[CrossRef](#)]
30. Tanaka, Y.; Nakai, T.; Matsushita, H.; Niwa, T. Experimental study on grooving corrosion occurring on welded joints for ship structure. *J. Jpn. Soc. Nav. Archit. Ocean Eng.* **2007**, *5*, 261–268.
31. Woloszyk, K.; Garbatov, Y. Advances in modelling and analysis of strength of corroded ship structures. *J. Mar. Sci. Eng.* **2022**, *10*, 807. [[CrossRef](#)]
32. Tsagris, M.; Beneki, C.; Hassani, H. On the folded normal distribution. *Mathematics* **2014**, *2*, 12–28. [[CrossRef](#)]
33. Gkatzogiannis, S.; Weinert, J.; Engelhardt, I.; Knoedel, P.; Ummenhofer, T. Correlation of laboratory and real marine corrosion for the investigation of corrosion fatigue behaviour of steel components. *Int. J. Fatigue* **2019**, *126*, 90–102. [[CrossRef](#)]
34. Xia, R.; Jia, C.; Liu, C.; Liu, P.; Zhang, S. Non-uniform corrosion characteristics of the steel pipe pile exposed to marine environments. *Ocean Eng.* **2023**, *272*, 113873. [[CrossRef](#)]

Disclaimer/Publisher’s Note: The statements, opinions and data contained in all publications are solely those of the individual author(s) and contributor(s) and not of MDPI and/or the editor(s). MDPI and/or the editor(s) disclaim responsibility for any injury to people or property resulting from any ideas, methods, instructions or products referred to in the content.